Available online at www.sciencedirect.com
ScienceDirect
Journal of Sound and Vibration 306 (2007) 91–110
JOURNAL OF SOUND AND VIBRATION
www.elsevier.com/locate/jsvi

Dynamic response of an infinite beam overlying a layered poroelastic half-space to moving loads

Bin Xu[a], Jian-Fei Lu[b,*], Jian-Hua Wang[a]

[a]Department of Civil Engineering, Shanghai JiaoTong University, Shanghai 200030, China
[b]Department of Civil Engineering, Jiangsu University, Zhenjiang, Jiangsu 212013, China

Received 23 February 2007; received in revised form 15 May 2007; accepted 19 May 2007
Available online 5 July 2007

Abstract

Dynamic response of an infinite beam resting on a layered poroelastic half-space subjected to moving loads is investigated in this study. The equivalent stiffness of the layered poroelastic half-space is obtained via the transmission and reflection matrices (TRM) method in the frequency wavenumber domain. Based on the obtained equivalent stiffness, the frequency wavenumber domain solution of the beam–half-space system is obtained by the compatibility condition between the beam and the half-space. The time domain solution for the beam and the layered half-space is obtained by means of the inverse Fourier transform method. Also, the influences of the load speed and material parameters of the poroelastic half-space on the responses of the beam as well as the layered half-space are investigated. In order to demonstrate the proposed method, some time–space domain examples and corresponding analysis are presented in the paper.

1. Introduction

Dynamic response of an infinite beam resting on a half-space under moving loads has been a topic for engineering society for a long time, as the model can be used to simulate the railway subjected to moving train loads or various pavements subjected to moving vehicle loads. Majority of the papers addressing the dynamic response of an infinite beam on a half-space to moving loads treat the half-space as an elastic or a visco-elastic medium. For example, the steady-state vibration of a beam supported on an elastic half-space under a moving load has been studied in Refs. [1–5]. The dynamic response of beams on the generalized Pasternak visco-elastic foundations subjected to an arbitrary distributed harmonic moving load was analyzed in Ref. [6]. The response of an elastic beam on a viscoelastic layer to a uniformly moving constant load is investigated in Refs. [7,8].

Recently some researchers have realized that high-speed trains will generate larger response for the rail and the ground especially for saturated soils, which may further cause noticeable structure-borne noise and vibration in the nearby buildings [9–11]. It is well known that the saturated soil is a two-phase material consisting of the soil skeleton and the pore water. Consequently, for a saturated soil, a saturated poroelastic

*Corresponding author.
E-mail addresses: xubin1@sjtu.edu.cn (B. Xu), ljfdoctor@yahoo.com (J.-F. Lu), wjh417@sjtu.edu.cn (J.-H. Wang).

0022-460X/$ - see front matter © 2007 Published by Elsevier Ltd.
doi:10.1016/j.jsv.2007.05.031

model is more realistic than the linear elastic or the visco-elastic one. Biot [12–14] pioneered the development of the theory for the saturated porous medium. Biot's theory has been widely applied in geomechanics to analyze consolidation effects due to quasi-static loads and wave propagation problems for dynamic loads.

It has been found that most foundations consist of several layers. Thus, a layered half-space is an appropriate model for inhomogeneous soils. It is worth pointing out that the dynamic response of a layered half-space to external loads has been investigated for a very long time. A review of the literature about the treatment of a layered half-space is given in Ref. [15]. It should be noticed that the transmission and reflection matrix (TRM) method established by Luco and Apsel [16,17] is a very important method for solving dynamic problems of a layered half-space. The advantage of the method is that the mismatched exponential terms are eliminated in all the terms of the TRM. As a result, the TRM method is valid even for high frequency and large layer thickness cases, which are difficult to solve by the typical propagator matrix method. Consequently, the TRM method has been used widely in solving layered structure problems [15–19]. To date, the research concerning a layered half-space has been mainly restricted to the elastic case, while the investigation about the layered porous medium is in a preliminary stage. Moreover, to the best of the authors' knowledge, study addressing the dynamic response of an infinite beam on a layered poroelastic half-space to moving loads is still unavailable in the literature.

In this paper the response of an infinite beam on a layered poroelastic half-space to a moving load is studied. The speed of the moving load is assumed to be a constant. Euler–Bernoulli beam theory is used to describe the beam, while Biot's theory is used to characterize the layered poroelastic half-space. The general solutions for the displacements, the stresses and the pore pressure of the layered half-space are established by solving Biot's dynamic equations via the Fourier transform method. Based on the continuity condition between the beam and the layered half-space as well as the continuity conditions at each layer interface, the TRM method is formulated to obtain the equivalent stiffness of the layered porous half-space. Using the expression for the equivalent stiffness of the layered porous half-space, the solutions for the beam and the layered poroelastic half-space are derived in the frequency-wavenumber domain. By means of the inverse Fourier transform, the time domain solutions for the beam and the poroelastic half-space are retrieved from the frequency-wavenumber solutions. When reduced to special cases, our solutions agree very well with some known results. The effects of load velocity, parameters of the poroelastic half-space on the deflection, the bending moment and the shear force of the beam as well as the response of the layered half-space are discussed.

2. Biot's theory and the corresponding general solution

The constitutive relations for the porous medium have the form [14]

$$\sigma_{ij} = \lambda\delta_{ij}\theta + 2\mu\varepsilon_{ij} - \alpha\delta_{ij}p, \tag{1}$$

$$p = -\alpha M\theta + Me, \tag{2}$$

$$e = -w_{i,i}, \quad \theta = u_{i,i}, \tag{3}$$

where u_i and w_i ($i = 1, 2, 3$) are the displacement of the solid skeleton and the infiltration displacement of the pore fluid, respectively; σ_{ij} is the stress of the bulk material; p is the pore pressure; ε_{ij} and θ are the strain tensor and the dilatation of the solid skeleton, respectively; e is the volume of fluid injected into a unit volume bulk material; δ_{ij} is the Kronecher delta; λ and μ are Lame constants; α and M are Biot's parameters accounting for compressibility of the porous medium.

The equations of motion for the bulk porous medium and the pore fluid have the form

$$\mu u_{i,jj} + (\lambda + \alpha^2 M + \mu)u_{j,ji} - \alpha M w_{j,ji} = \rho\ddot{u}_i + \rho_f\ddot{w}_i, \tag{4a}$$

$$\alpha M u_{j,ji} + M w_{j,ji} = \rho_f\ddot{u}_i + m\ddot{w}_i + b_p K(t)*\dot{w}_i, \tag{4b}$$

where ρ and ρ_f are mass densities of the bulk material and the pore fluid, $\rho = (1-f)\rho_s + f\rho_f$, ρ_s is the density of the solid skeleton and f is the porosity of the porous medium; $m = a_\infty\rho_f/f$ and a_∞ is tortuosity; b_p accounts for the viscosity of the pore fluid and the permeability of the porous medium, respectively and $K(t)$ is

a time-dependent viscosity correction factor which describes the transition behavior from viscosity dominated flow in the low frequency range towards inertia dominated flow at high-frequency range [20]; the dot over a variable denotes the time derivative and a star (∗) between the two variables denotes the time convolution.

In order to solve Biot's governing equations, two kinds of Fourier transform are involved: the Fourier transform with respect to time and frequency and the Fourier transform with respect to horizontal coordinates and horizontal wavenumbers. In this paper, the Fourier transform for time and the two horizontal coordinates are defined as follows:

$$\hat{f}(\omega)=\int_{-\infty}^{\infty} f(t)\mathrm{e}^{-\mathrm{i}\omega t}\,\mathrm{d}t,\quad f(t)=\frac{1}{2\pi}\int_{-\infty}^{\infty}\hat{f}(\omega)\mathrm{e}^{\mathrm{i}\omega t}\,\mathrm{d}\omega,$$

$$\bar{f}(\xi)=\int_{-\infty}^{\infty} f(x)\mathrm{e}^{-\mathrm{i}\xi x}\,\mathrm{d}x,\quad f(x)=\frac{1}{2\pi}\int_{-\infty}^{\infty}\bar{f}(\xi)\mathrm{e}^{\mathrm{i}\xi x}\,\mathrm{d}\xi,$$

$$\tilde{f}(\eta)=\int_{-\infty}^{\infty} f(y)\mathrm{e}^{-\mathrm{i}\eta y}\,\mathrm{d}y,\quad f(y)=\frac{1}{2\pi}\int_{-\infty}^{\infty}\tilde{f}(\eta)\mathrm{e}^{\mathrm{i}\eta y}\,\mathrm{d}\eta, \tag{5}$$

where the superimposed symbols $\hat{}$, $-$ and $\sim$ above a variable denote the Fourier transform with respect to time t, x and y coordinates, respectively.

Performing the Fourier transform with respect to time t on Eqs. (2) and (4b), the infiltration displacement of the pore fluid has the form

$$\hat{w}_j=\frac{\hat{p}_{,j}}{m\omega^2-\mathrm{i}b_p\hat{K}(\omega)\omega}-\vartheta\hat{u}_j\quad(j=1,2,3), \tag{6}$$

where $\vartheta=\rho_f\omega^2/[m\omega^2-\mathrm{i}b_p\hat{K}(\omega)\omega]$.

Substituting Eq. (6) into Eq. (4a), one has the following equation:

$$\mu\hat{u}_{i,jj}+(\lambda+\mu)\hat{u}_{j,ji}+\omega^2(\rho-\rho_f\vartheta)\hat{u}_i-(\alpha-\vartheta)\hat{p}_{,i}=0. \tag{7}$$

Applying the divergence operator on Eq. (6) and substituting the resulting divergence and Eq. (3) into Eq. (2), the following equation is obtained:

$$\nabla^2\hat{p}+\frac{\rho_f\omega^2}{\vartheta M}\hat{p}+\rho_f\omega^2(\alpha-\vartheta)\frac{\hat{\theta}}{\vartheta}=0. \tag{8}$$

Likewise, applying the divergence operator on the frequency domain expression of Eq. (4a), the following equation is obtained:

$$(\lambda+\alpha^2M+2\mu)\nabla^2\hat{\theta}+\omega^2(\rho-\rho_f\vartheta)\hat{\theta}-(\alpha-\vartheta)\nabla^2\hat{p}=0. \tag{9}$$

From Eq. (8), one has the following equation:

$$\hat{\theta}=-\frac{\vartheta\nabla^2\hat{p}}{\rho_f\omega^2(\alpha-\vartheta)}-\frac{\hat{p}}{(\alpha-\vartheta)M}. \tag{10}$$

Substitution of Eq. (10) into Eq. (9) yields the following equation:

$$\nabla^4\hat{p}+\beta_1\nabla^2\hat{p}+\beta_2\hat{p}=0, \tag{11}$$

where $\beta_1=[(m\omega^2-\mathrm{i}b_p\hat{K}(\omega)\omega)(\lambda+\alpha^2M+2\mu)+\rho\omega^2M-2\alpha M\rho_f\omega^2]/[(\lambda+2\mu)M]$, $\beta_2=[(m\omega^2-\mathrm{i}b_p\hat{K}(\omega)\omega)\rho\omega^2M-\rho_f^2\omega^4]/[(\lambda+2\mu)M]$.

Performing the double Fourier transform with respect to the two horizontal coordinates x and y on Eq. (11) and solving the resulting ordinary differential equation lead to

$$\tilde{\hat{p}}=A\mathrm{e}^{\gamma_1 z}+B\mathrm{e}^{-\gamma_1 z}+C\mathrm{e}^{\gamma_2 z}+D\mathrm{e}^{-\gamma_2 z}, \tag{12}$$

where $\gamma_j=\sqrt{\xi^2+\eta^2-\ell_j^2}$, $\ell_1^2=\frac{1}{2}\left(\beta_1-\sqrt{\beta_1^2-4\beta_2}\right)$, $\ell_2^2=\frac{1}{2}\left(\beta_1+\sqrt{\beta_1^2-4\beta_2}\right)$ $(j=1,\ 2)$, ℓ_1 and ℓ_2 are the complex wavenumbers for the first kind (fast wave) and the second kind (slow wave) dilatational wave, respectively. Note that the radicals γ_i $(i=1,\ 2)$ are selected such that $\mathrm{Re}(\gamma_i)\geqslant 0$.

Performing the double Fourier integral transform with respect to the two horizontal coordinates x and y on Eq. (10) and substituting Eq. (12) into the resulting equation yield

$$\hat{\tilde{\theta}} = \chi_1(A\mathrm{e}^{\gamma_1 z} + B\mathrm{e}^{-\gamma_1 z}) + \chi_2(C\mathrm{e}^{\gamma_2 z} + D\mathrm{e}^{-\gamma_2 z}), \tag{13}$$

where $\chi_j = [\vartheta M \ell_j^2 - \rho_f \omega^2]/[\rho_f \omega^2(\alpha - \vartheta)M]$ $(j = 1, 2)$.

Substituting $\hat{\tilde{p}}(\xi, \eta, z, \omega)$ and $\hat{\tilde{\theta}}(\xi, \eta, z, \omega)$ into the transformed form of Eq. (4), one has

$$\hat{\tilde{u}}_y = -\mathrm{i}\eta[a_1(A\mathrm{e}^{\gamma_1 z} + B\mathrm{e}^{-\gamma_1 z}) + a_2(C\mathrm{e}^{\gamma_2 z} + D\mathrm{e}^{-\gamma_2 z})] + G\mathrm{e}^{\gamma_3 z} + H\mathrm{e}^{-\gamma_3 z},$$

$$\hat{\tilde{u}}_z = -\gamma_1 a_1(A\mathrm{e}^{\gamma_1 z} - B\mathrm{e}^{-\gamma_1 z}) - \gamma_2 a_2(C\mathrm{e}^{\gamma_2 z} - D\mathrm{e}^{-\gamma_2 z}) + E\mathrm{e}^{\gamma_3 z} + F\mathrm{e}^{-\gamma_3 z},$$

$$\hat{\tilde{w}}_z = \gamma_1(a_1\vartheta + \rho_f\omega^2/\vartheta)(A\mathrm{e}^{\gamma_1 z} - B\mathrm{e}^{-\gamma_1 z}) + \gamma_2(a_2\vartheta + \rho_f\omega^2/\vartheta)(C\mathrm{e}^{\gamma_2 z} - D\mathrm{e}^{-\gamma_2 z}) - \vartheta(E\mathrm{e}^{\gamma_3 z} + F\mathrm{e}^{-\gamma_3 z}), \tag{14}$$

where $a_j = [\lambda(\chi_j + \mu) - \alpha + \vartheta]/[(S^2 - \ell_j^2)\mu]$ $(j = 1, 2)$, $S^2 = (\rho - \rho_f\vartheta)\omega^2/\mu$, $\gamma_3 = \sqrt{\xi^2 + \eta^2 - S^2}$, S is the complex wavenumber for the shear wave and $A, B, C, \ldots, H$ are arbitrary constants. Note that the radical γ_3 is selected such that $\mathrm{Re}(\gamma_3) \geqslant 0$.

Using the transformed expression for the dilatation of the solid

$$\hat{\tilde{\theta}} = i\xi\hat{\tilde{u}}_x + \mathrm{i}\eta\hat{\tilde{u}}_y + \partial\hat{\tilde{u}}_z/\partial z, \tag{15}$$

$\hat{\tilde{u}}_x$ is obtained as follows:

$$\mathrm{i}\xi\hat{\tilde{u}}_x = v_1(A\mathrm{e}^{\gamma_1 z} + B\mathrm{e}^{-\gamma_1 z}) + v_2(C\mathrm{e}^{\gamma_2 z} + D\mathrm{e}^{-\gamma_2 z}) - \gamma_3(E\mathrm{e}^{\gamma_3 z} - F\mathrm{e}^{-\gamma_3 z}) - \mathrm{i}\eta(G\mathrm{e}^{\gamma_3 z} + H\mathrm{e}^{-\gamma_3 z}). \tag{16}$$

In terms of Eqs. (1) and (2), the following stresses are obtained:

$$\mathrm{i}\xi\hat{\tilde{\sigma}}_{xz} = -g_1(\mathrm{A}\mathrm{e}^{\gamma_1 z} - \mathrm{B}\mathrm{e}^{-\gamma_1 z}) - g_2(\mathrm{C}\mathrm{e}^{\gamma_2 z} - \mathrm{D}\mathrm{e}^{-\gamma_2 z}) - (\xi^2 + \gamma_3^2)(\mathrm{E}\mathrm{e}^{\gamma_3 z} + \mathrm{F}\mathrm{e}^{-\gamma_3 z}) - \mathrm{i}\gamma_3\eta(\mathrm{G}\mathrm{e}^{\gamma_3 z} - \mathrm{H}\mathrm{e}^{-\gamma_3 z}),$$

$$\hat{\tilde{\sigma}}_{yz} = -2\mathrm{i}\eta\gamma_1 a_1(A\mathrm{e}^{\gamma_1 z} - B\mathrm{e}^{-\gamma_1 z}) - 2\mathrm{i}\eta\gamma_2 a_2(C\mathrm{e}^{\gamma_2 z} - D\mathrm{e}^{-\gamma_2 z}) + \mathrm{i}\eta(E\mathrm{e}^{\gamma_3 z} + F\mathrm{e}^{-\gamma_3 z}) + \gamma_3(G\mathrm{e}^{\gamma_3 z} - H\mathrm{e}^{-\gamma_3 z}),$$

$$\hat{\tilde{\sigma}}_{zz} = \tau_1(A\mathrm{e}^{\gamma_1 z} + B\mathrm{e}^{-\gamma_1 z}) + \tau_2(C\mathrm{e}^{\gamma_2 z} + D\mathrm{e}^{-\gamma_2 z}) + 2\mu\gamma_3(E\mathrm{e}^{\gamma_3 z} - F\mathrm{e}^{-\gamma_3 z}), \tag{17}$$

where $g_j = \chi_j + a_j(\gamma_j^2 - \eta^2)$, $\tau_i = \lambda(\chi_j - 2\mu a_j\gamma_j^2)$, $v_j = -\gamma_j\left[\chi_j + a_j(\gamma_j^2 + \xi^2 - \eta^2)\right]$ $(j = 1, 2)$.

3. The model for a beam resting on a layered poroelastic half-space subjected to a moving load

Fig. 1 illustrates an infinite Euler–Bernoulli beam resting on a layered poroelastic half-space and subjected to a moving load with a constant velocity. For simplicity, the following assumptions are made for the beam and the load: (a) the beam is treated as an infinite Euler–Bernoulli elastic beam with a width $2a$; (b) the deformation of the beam is infinitesimal; (c) the shear deformation and the rotary inertia of the beam are negligible; (d) both the moving load and the normal stresses between the beam and the half-space are uniformly distributed over the width of the beam; (e) the contact between the beam and the half-space is smooth.

According to the elastic beam theory, the equation of motion for the beam is as follows:

$$EI_z\frac{\partial^4 w_b(x,t)}{\partial^4 x} + m_b\frac{\partial^2 w_b(x,t)}{\partial^2 t} = F(x,t) - q_z(x,t), \tag{18}$$

where $w_b(x, t)$ is the deflection of the beam, E Young's modulus of beam material, I_z the second moment of area of the beam cross section about its neutral axis (Fig. 1), $q_z(x, t)$ is the interaction force between the beam and the half-space, $F(x, t)$ is the applied moving load which is uniformly distributed over the width. The moving load $F(x, t)$ is a line load moving with a constant velocity c and given by the following expression:

$$F(x,t) = F_z\delta(x - ct), \tag{19}$$

where F_z is the magnitude of the load, $\delta(\cdots)$ is the Dirac delta function.

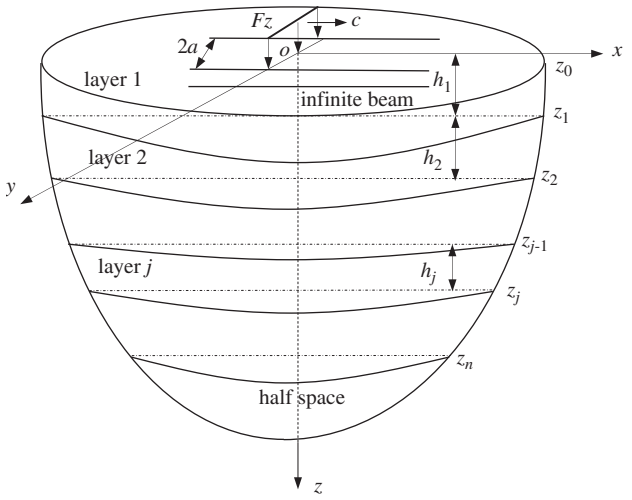

Fig. 1. An infinite beam overlying a layered poroelastic half-space subjected to moving loads.

According to the assumptions concerning the beam, the stress boundary conditions for the surface of the layered half-space are as follows:

$$2a\sigma_{zz}(x,y,0,t) = q_z(x,t)H(a-|y|),$$

$$\sigma_{xz}(x,y,0,t) = 0, \quad \sigma_{yz}(x,y,0,t) = 0, \tag{20}$$

where $H(\cdots)$ is the unit step function. Moreover, the following "open pore" boundary conditions is assumed for the surface of the poroelastic half-space [21]

$$p(x,y,0,t) = 0. \tag{21}$$

Assuming that the centerline of the beam and the surface of the half-space are always in contact, then, the following compatibility condition holds:

$$u_z(x,0,0,t) = w_b(x,t). \tag{22}$$

To calculate the bending moment and the shear force for the beam, the following relations are used:

$$M_x(x,t) = EI_z\frac{\partial^2 w_b(x,t)}{\partial^2 x},$$

$$Q_x(x,t) = EI_z\frac{\partial^3 w_b(x,t)}{\partial^3 x}. \tag{23}$$

Fourier transformation of Eqs. (19) and (23) with respect to the coordinate x and use of the shifting theorem of the Fourier transform yield the following relations:

$$\hat{\tilde{F}}(\xi,\omega) = 2\pi F_z\delta(\omega+\xi c), \tag{24}$$

$$\hat{\tilde{M}}_x(\xi,\omega) = -EI_z\xi^2\hat{\tilde{w}}_b(\xi,\omega), \tag{25a}$$

$$\hat{\tilde{Q}}_x(\xi,\omega) = -\mathrm{i}EI_z\xi^3\hat{\tilde{w}}_b(\xi,\omega). \tag{25b}$$

4. TRM method for a beam overlying a layered poroelastic half-space

The model for an infinite beam resting on n horizontal porous layers overlying a porous half-space is illustrated in Fig. 1. The jth porous layer is denoted by the symbol L_j and the bottom layer is denoted by L_{n+1}. The thickness of the jth layer is $h_j = z_j - z_{j-1}$ and z_{j-1}, z_j are the depth of the upper and lower boundary of the jth layer. To solve the beam and the half-space system, the concept of the "equivalent stiffness" [7] is introduced for the half-space. The equivalent stiffness method allows an exact reduction of an original 3-D problem to a 1-D problem by introducing a frequency and wavenumber-dependent complex stiffness k_{eq} for the layered half-space.

To determine the equivalent stiffness for the layered porous half-space, the TRM formulation for a layered porous half-space is necessary. Extracting all the positive and negative exponential term $\mathrm{e}^{\pm\gamma_i z}(i = 1, 2, 3)$ from general solution for the displacements, the pore pressure and the stresses (Eqs. (12), (14), (16), (17)) of the jth porous layer L_j and combining them with the arbitrary functions $A(\xi, \eta, \omega), \ldots, H(\xi, \eta, \omega)$, which are replaced by $a^{(j)}(\xi,\eta,\omega)\mathrm{e}^{-\gamma_{1j}z_j}$,$b^{(j)}(\xi,\eta,\omega)\mathrm{e}^{\gamma_{1j}z_{j-1}}$, $c^{(j)}(\xi,\eta,\omega)\mathrm{e}^{-\gamma_{2j}z_j}$,$d^{(j)}(\xi,\eta,\omega)\mathrm{e}^{\gamma_{2j}z_{j-1}}$, $e^{(j)}(\xi,\eta,\omega)\mathrm{e}^{-\gamma_{3j}z_j}$, $f^{(j)}(\xi,\eta,\omega)\mathrm{e}^{\gamma_{3j}z_{j-1}}$, $g^{(j)}(\xi,\eta,\omega)\mathrm{e}^{-\gamma_{3j}z_j}$, $h^{(j)}(\xi,\eta,\omega)\mathrm{e}^{\gamma_{3j}z_{j-1}}$, respectively, the expressions for the displacements, the stresses and the pore pressure for the jth porous layer have the following form:

$$\mathbf{\Psi}^{(j)}(\xi,\eta,\omega,z)_{8\times1} = \begin{bmatrix} \mathbf{D}_d^{(j)}(\xi,\eta,\omega) & \mathbf{D}_u^{(j)}(\xi,\eta,\omega) \\ \mathbf{S}_d^{(j)}(\xi,\eta,\omega) & \mathbf{S}_u^{(j)}(\xi,\eta,\omega) \end{bmatrix} \times \left[\mathbf{W}_d^{(j)}(\xi,\eta,\omega,z)^{\mathrm{T}}\mathbf{W}_u^{(j)}(\xi,\eta,\omega,z)^{\mathrm{T}}\right]^{\mathrm{T}}, \tag{26a}$$

$$\mathbf{\Psi}^{(j)}(\xi,\eta,\omega,z)_{8\times1} = \left[\mathrm{i}\xi\tilde{\tilde{u}}_x^{(j)}\ \tilde{\tilde{u}}_y^{(j)}\ \tilde{\tilde{u}}_z^{(j)}\ \tilde{\tilde{w}}_z^{(j)}\ \mathrm{i}\xi\tilde{\tilde{\sigma}}_{xz}^{(j)}\ \tilde{\tilde{\sigma}}_{yz}^{(j)}\ \tilde{\tilde{\sigma}}_{zz}^{(j)}\ \tilde{\tilde{p}}^{(j)}\right]^{\mathrm{T}}, \tag{26b}$$

$$\mathbf{W}_d^{(j)}(\xi,\eta,\omega,z) = \left[b^{(j)}\mathrm{e}^{-\gamma_{1j}(z-z_{j-1})}\ d^{(j)}\mathrm{e}^{-\gamma_{2j}(z-z_{j-1})}\ f^{(j)}\mathrm{e}^{-\gamma_{3j}(z-z_{j-1})}\ h^{(j)}\mathrm{e}^{-\gamma_{3j}(z-z_{j-1})}\right]^{\mathrm{T}}, \tag{26c}$$

$$\mathbf{W}_u^{(j)}(\xi,\eta,\omega,z) = \left[a^{(j)}\mathrm{e}^{-\gamma_{1j}(z_j-z)}\ c^{(j)}\mathrm{e}^{-\gamma_{2j}(z_j-z)}\ e^{(j)}\mathrm{e}^{-\gamma_{3j}(z_j-z)}\ g^{(j)}\mathrm{e}^{-\gamma_{3j}(z_j-z)}\right]^{\mathrm{T}}, \tag{26d}$$

where the superscript j denotes the jth porous layer and $\mathbf{\Psi}^{(j)}(\xi,\eta,z,\omega)_{8\times1}$ is the vector for the displacements, the stresses and the pore pressure in the frequency–wavenumber domain. Note that the vectors $\mathbf{W}_d^{(j)}(\xi,\eta,z,\omega)$, $\mathbf{W}_u^{(j)}(\xi,\eta,z,\omega)$ are termed as down-going and up-going wave vector.

From Eqs. (26c) and (26d), one has the following equations:

$$\mathbf{W}_d^{(j)}(\xi,\eta,z_{j-1},\omega) = \left[b^{(j)}(\xi,\eta,\omega)\ d^{(j)}(\xi,\eta,\omega)\ f^{(j)}(\xi,\eta,\omega)\ h^{(j)}(\xi,\eta,\omega)\right]^{\mathrm{T}},$$

$$\mathbf{W}_u^{(j)}(\xi,\eta,z_j,\omega) = \left[a^{(j)}(\xi,\eta,\omega)\ c^{(j)}(\xi,\eta,\omega)\ e^{(j)}(\xi,\eta,\omega)\ g^{(j)}(\xi,\eta,\omega)\right]^{\mathrm{T}}. \tag{27}$$

In terms of Eqs. (26) and (27), the down-going and the up-going wave vectors are recast in the following form:

$$\mathbf{W}_d^{(j)}(\xi,\eta,z,\omega) = \mathbf{E}^{(j)}(z - z_{j-1})\mathbf{W}_d^{(j)}(\xi,\eta,z_{j-1},\omega),$$

$$\mathbf{W}_u^{(j)}(\xi,\eta,z,\omega) = \mathbf{E}^{(j)}(z_j - z)\mathbf{W}_u^{(j)}(\xi,\eta,z_j,\omega), \tag{28}$$

where

$$\mathbf{E}^{(j)}(\hbar) = \begin{bmatrix} \mathrm{e}^{-\gamma_{1j}\hbar} & 0 & 0 & 0 \\ 0 & \mathrm{e}^{-\gamma_{2j}\hbar} & 0 & 0 \\ 0 & 0 & \mathrm{e}^{-\gamma_{3j}\hbar} & 0 \\ 0 & 0 & 0 & \mathrm{e}^{-\gamma_{3j}\hbar} \end{bmatrix}.$$

According to Deresiewicz and Skalak [21], displacements u_x, u_y, u_z, w_z and the pore pressure p, stresses σ_{xz}, σ_{yz}, σ_{zz} should be continuous at the interfaces. Thus, the following eight continuity conditions

hold at each interface:

$$\hat{\tilde{u}}_x^{(j)}(\xi,\eta,z_j,\omega)=\hat{\tilde{u}}_x^{(j+1)}(\xi,\eta,z_j,\omega),\quad \hat{\tilde{u}}_y^{(j)}(\xi,\eta,z_j,\omega)=\hat{\tilde{u}}_y^{(j+1)}(\xi,\eta,z_j,\omega),$$

$$\hat{\tilde{u}}_z^{(j)}(\xi,\eta,z_j,\omega)=\hat{\tilde{u}}_z^{(j+1)}(\xi,\eta,z_j,\omega),\quad \hat{\tilde{p}}^{(j)}(\xi,\eta,z_j,\omega)=\hat{\tilde{p}}^{(j+1)}(\xi,\eta,z_j,\omega),$$

$$\hat{\tilde{\sigma}}_{xz}^{(j)}(\xi,\eta,z_j,\omega)=\hat{\tilde{\sigma}}_{xz}^{(j+1)}(\xi,\eta,z_j,\omega),\quad \hat{\tilde{\sigma}}_{yz}^{(j)}(\xi,\eta,z_j,\omega)=\hat{\tilde{\sigma}}_{yz}^{(j+1)}(\xi,\eta,z_j,\omega),$$

$$\hat{\tilde{\sigma}}_{zz}^{(j)}(\xi,\eta,z_j,\omega)=\hat{\tilde{\sigma}}_{zz}^{(j+1)}(\xi,\eta,z_j,\omega),\quad \hat{\tilde{w}}_z^{(j)}(\xi,\eta,z_j,\omega)=\hat{\tilde{w}}_z^{(j+1)}(\xi,\eta,z_j,\omega)\ (j=1,2,\ldots,n). \tag{29}$$

Besides, if the bottom layer (L_{n+1} layer) is a half-space, the up-going wave should vanish. One, therefore, has the following four radiation conditions:

$$\mathbf{W}_u^{(n+1)}(\xi,\eta,z,\omega)=0,\quad z\in L_{n+1}. \tag{30}$$

If the layered half-space consists of n porous layers overlying a rigid half-space with a completely impermeable surface, then, the boundary condition for the nth layer at $z=z_n$ has the following form:

$$\hat{\tilde{u}}_x^{(n)}(\xi,\eta,z_n,\omega)=0,\quad \hat{\tilde{u}}_y^{(n)}\,\xi,\eta,z_n,\omega)=0,$$

$$\hat{\tilde{u}}_z^{(n)}(\xi,\eta,z_n,\omega)=0,\quad \hat{\tilde{w}}_z^{(n)}(\xi,\eta,z_n,\omega)=0. \tag{31}$$

In terms of Eq. (26), the continuity condition (29) for the jth interface is recast as follows:

$$\begin{bmatrix}-\mathbf{D}_d^{(j+1)} & \mathbf{D}_u^{(j)}\\ -\mathbf{S}_d^{(j+1)} & \mathbf{S}_u^{(j)}\end{bmatrix}\begin{bmatrix}\mathbf{W}_d^{(j+1)}(\xi,\eta,\omega,z_j)\\ \mathbf{W}_u^{(j)}(\xi,\eta,\omega,z_j)\end{bmatrix}=\begin{bmatrix}-\mathbf{D}_d^{(j)} & \mathbf{D}_u^{(j+1)}\\ -\mathbf{S}_d^{(j)} & \mathbf{S}_u^{(j+1)}\end{bmatrix}\begin{bmatrix}\mathbf{W}_d^{(j)}(\xi,\eta,\omega,z_j)\\ \mathbf{W}_u^{(j+1)}(\xi,\eta,\omega,z_j)\end{bmatrix}\quad (j=1,2,\ldots,n). \tag{32}$$

Inversion of the matrix at the left-hand side of Eq. (32) gives

$$\begin{bmatrix}\mathbf{W}_d^{(j+1)}(\xi,\eta,\omega,z_j)\\ \mathbf{W}_u^{(j)}(\xi,\eta,\omega,z_j)\end{bmatrix}=\begin{bmatrix}\mathbf{T}_d^{(j)} & \mathbf{R}_u^{(j)}\\ \mathbf{R}_d^{(j)} & \mathbf{T}_u^{(j)}\end{bmatrix}\begin{bmatrix}\mathbf{W}_d^{(j)}(\xi,\eta,\omega,z_j)\\ \mathbf{W}_u^{(j+1)}(\xi,\eta,\omega,z_j)\end{bmatrix}, \tag{33}$$

where

$$\begin{bmatrix}\mathbf{T}_d^{(j)} & \mathbf{R}_u^{(j)}\\ \mathbf{R}_d^{(j)} & \mathbf{T}_u^{(j)}\end{bmatrix}=\begin{bmatrix}-\mathbf{D}_d^{(j+1)} & \mathbf{D}_u^{(j)}\\ -\mathbf{S}_d^{(j+1)} & \mathbf{S}_u^{(j)}\end{bmatrix}^{-1}\begin{bmatrix}-\mathbf{D}_d^{(j)} & \mathbf{D}_u^{(j+1)}\\ -\mathbf{S}_d^{(j)} & \mathbf{S}_u^{(j+1)}\end{bmatrix}.$$

The 4×4 matrix $\mathbf{R}_u^{(j)}(\xi,\eta,\omega)$ and $\mathbf{R}_d^{(j)}(\xi,\eta,\omega)$ in Eq. (33) represent reflection matrices for the up-going and the down-going $P1$, $P2$, S waves incident on the jth interface, while $\mathbf{T}_u^{(j)}(\xi,\eta,\omega)$, $\mathbf{T}_d^{(j)}(\xi,\eta,\omega)$ denote the transmission matrices for the up-going and the down-going $P1$, $P2$, S waves incident on the jth interface.

For simplicity, the following matrix notations are introduced:

$$\begin{bmatrix}\mathbf{T}_{de}^{(j)} & \mathbf{R}_{ue}^{(j)}\\ \mathbf{R}_{de}^{(j)} & \mathbf{T}_{ue}^{(j)}\end{bmatrix}=\begin{bmatrix}\mathbf{T}_d^{(j)} & \mathbf{R}_u^{(j)}\\ \mathbf{R}_d^{(j)} & \mathbf{T}_u^{(j)}\end{bmatrix}\begin{bmatrix}\mathbf{E}^{(j)}(h_j) & 0\\ 0 & \mathbf{E}^{(j+1)}(h_{j+1})\end{bmatrix},$$

$$\begin{bmatrix}\mathbf{T}_{de}^{g(j)} & \mathbf{R}_{ue}^{g(j)}\\ \mathbf{R}_{de}^{g(j)} & \mathbf{T}_{ue}^{g(j)}\end{bmatrix}=\begin{bmatrix}\mathbf{T}_d^{g(j)} & \mathbf{R}_u^{g(j)}\\ \mathbf{R}_d^{g(j)} & \mathbf{T}_u^{g(j)}\end{bmatrix}\begin{bmatrix}\mathbf{E}^{(j)}(h_j) & 0\\ 0 & \mathbf{E}^{(j+1)}(h_{j+1})\end{bmatrix}, \tag{34}$$

where $\mathbf{T}_{de}^{g(j)}(\xi,\eta,\omega)$, $\mathbf{R}_{de}^{g(j)}(\xi,\eta,\omega)$, $\mathbf{T}_{ue}^{g(j)}(\xi,\eta,\omega)$,$\mathbf{R}_{ue}^{g(j)}(\xi,\eta,\omega)$ are the generalized transmission and reflection matrices for the down-going and the up-going wave incident on the jth interface and their expressions will be given below.

According to Lu and Hanyga [15], the following equations connecting the downward wave vector $\mathbf{W}_d^{(1)}(\xi,\eta,0,\omega)$ in the first layer with the up-going and the down-going wave vectors $\mathbf{W}_u^{(j)}(\xi,\eta,z_j,\omega)$, $\mathbf{W}_d^{(j)}(\xi,\eta,z_{j-1},\omega)$ in the L_j $(j=1,2,\ldots,n)$ hold

$$\mathbf{W}_d^{(j)}(\xi,\eta,z_{j-1},\omega)=\mathbf{T}_{de}^{g(j-1)}\mathbf{T}_{de}^{g(j-2)}\cdots\mathbf{T}_{de}^{g(2)}\mathbf{T}_d^{g(1)}\mathbf{W}_d^{(1)}(\xi,\eta,z_1,\omega), \tag{35a}$$

$$\mathbf{W}_u^{(j)}(\xi,\eta,z_j,\omega)=\mathbf{R}_d^{g(j)}\mathbf{W}_d^{(j)}(\xi,\eta,z_j,\omega), \tag{35b}$$

$$\mathbf{R}_d^{g(j)}=\mathbf{R}_d^{(j)}+\mathbf{T}_{ue}^{(j)}\mathbf{R}_{de}^{(j+1)}\mathbf{T}_d^{g(j)}, \tag{35c}$$

$$\mathbf{T}_{de}^{g(j)}=(\mathbf{I}-\mathbf{R}_{ue}^{(j)}\mathbf{R}_{de}^{g(j+1)})^{-1}\mathbf{T}_{de}^{(j)},\quad j=1,2,\ldots,n. \tag{35d}$$

If the bottom layer has the radiation condition (30), the following relation is obtained from Eq. (33):

$$\mathbf{R}_{de}^{g(n+1)}=0. \tag{36}$$

On the other hand, if the bottom layer is a rigid half-space, in terms of Eq. (26), one has the following equation:

$$\mathbf{D}_d^{(n)}\mathbf{W}_d^{(n)}(\xi,\eta,\omega,z_n)+\mathbf{D}_u^{(n)}\mathbf{W}_u^{(n)}(\xi,\eta,\omega,z_n)=0. \tag{37}$$

From Eq. (37), one has the following equation:

$$\mathbf{W}_u^{(n)}(\xi,\eta,z_n,\omega)=\mathbf{R}_{de}^{g(n)}\mathbf{W}_d^{(n)}(\xi,\eta,z_{n-1},\omega), \tag{38}$$

where $\mathbf{R}_{de}^{g(n)}=-\left[\mathbf{D}_u^{(n)}\right]^{-1}\mathbf{D}_d^{(n)}\mathbf{E}(h_n)$.

Note that in terms of the known $\mathbf{R}_{de}^{g(n+1)}$ or $\mathbf{R}_{de}^{g(n)}$, $\mathbf{T}_d^{g(j)}$ and $\mathbf{R}_d^{g(j)}$ are available for each layer via Eq. (35). In terms of the surface boundary conditions Eqs. (20), (21) and (26), the following relation is obtained:

$$\mathbf{S}_d^{(1)}\mathbf{W}_d^{(1)}(\xi,\eta,0,\omega)+\mathbf{S}_u^{(1)}\mathbf{W}_u^{(1)}(\xi,\eta,0,\omega)=\hat{\tilde{\mathbf{Q}}}(\xi,\eta,\omega), \tag{39}$$

where $\hat{\tilde{\mathbf{Q}}}(\xi,\eta,\omega)=\left[0\;0-\sin(\eta a)/(\eta a)\hat{\tilde{q}}_z(\xi,\omega)\;0\right]^{\mathrm{T}}$.

According to Eq. (35b), the following equation is obtained:

$$\mathbf{W}_u^{(1)}(\xi,\eta,z_1,\omega)=\mathbf{R}_{de}^{g(1)}\mathbf{W}_d^{(1)}(\xi,\eta,0,\omega), \tag{40}$$

where $\mathbf{R}_{de}^{g(1)}$ can be obtained by Eq. (35). Substitutions of Eq. (40) into Eq. (39), the down-going wave vector for the first layer is obtained

$$\mathbf{W}_d^{(1)}(\xi,\eta,0,\omega)=[\mathbf{S}_d^{(1)}+\mathbf{S}_u^{(1)}\mathbf{E}^{(1)}(h_1)\mathbf{R}_{de}^{g(1)}]^{-1}\hat{\tilde{\mathbf{Q}}}(\xi,\eta,\omega). \tag{41}$$

Substitution of the wave vectors $\mathbf{W}_u^{(1)}(\xi,\eta,z_1,\omega)$ and $\mathbf{W}_d^{(1)}(\xi,\eta,0,\omega)$ for the first layer into Eq. (26a), the vertical displacement of the first layer is obtained as follows:

$$\hat{\tilde{u}}_z(\xi,\eta,0,\omega)=-\frac{\sin(\eta a)}{\eta a}\phi(\xi,\eta,0,\omega)\hat{\tilde{q}}_z(\xi,\omega), \tag{42}$$

where $\phi(\xi,\eta,0,\omega)$ can be obtained by Eqs. (26), (40) and (41).

Performing the inverse Fourier transform with respect to $\eta\to y$ on Eq. (42), one has the following equation:

$$\hat{u}_z(\xi,0,0,\omega)=\frac{\hat{\tilde{q}}_z(\xi,\omega)}{2\pi}\int_{-\infty}^{\infty}\frac{\sin(\eta a)}{\eta a}\phi(\xi,\eta,0,\omega)\,\mathrm{d}\eta. \tag{43}$$

Substituting Eq. (43), the compatibility condition (22) into Eq. (18) in the ξ, ω domain, one has the following equations for the beam in the Fourier transformed domain:

$$\hat{\tilde{w}}_b(\xi,\omega)=\frac{2\pi F_z\delta(\omega+\xi c)}{\left[-m_b\omega^2+EI_z\xi^4+k_{\mathrm{eq}}(\xi,\omega)\right]}, \tag{44}$$

$$k_{\mathrm{eq}}(\xi,\omega)=\frac{2\pi}{\int_{-\infty}^{\infty}\phi(\xi,\eta,0,\omega)[\sin(\eta a)/(\eta a)]\,\mathrm{d}\eta}, \tag{45}$$

where $k_{eq}(\xi, \omega)$ is the equivalent stiffness of the layered half-space. As mentioned above, the equivalent stiffness of the layered half-space is a function of the frequency ω and the wavenumber ξ.

5. Solution of the beam and the half-space system

Applying the two-dimensional inverse Fourier transformation for $\xi \to x$ and $\omega \to t$ on Eq. (44) and using the property of the Dirac's delta function, the following equation is obtained:

$$w_b(x,t) = \frac{F_z}{2\pi}\int_{-\infty}^{\infty} \frac{e^{i\xi x}}{EI\xi^4 - m_b(\xi c)^2 + k_{eq}(\xi, -\xi c)}\, d\xi. \tag{46}$$

The expressions for the bending moment and the shear force of the beam have the following form:

$$M_x(x,t) = -\frac{F_z}{2\pi}\int_{-\infty}^{\infty} \frac{EI_z\xi^2 e^{i\xi x}}{EI\xi^4 - m_b(\xi c)^2 + k_{eq}(\xi, -\xi c)}\, d\xi,$$

$$Q_x(x,t) = -\frac{iF_z}{2\pi}\int_{-\infty}^{\infty} \frac{EI_z\xi^3 e^{i\xi x}}{EI_z\xi^4 - m_b(\xi c)^2 + k_{eq}(\xi, -\xi c)}\, d\xi. \tag{47}$$

After determining the deflection of the beam via Eq. (44), the wave vectors for the first layer can be calculated by Eqs. (22), (40), (41) and (43). Based on the obtained wave vectors for the first layer, the up-going and the down-going wave vectors $\mathbf{W}_u^{(j)}(\xi, \eta, z_j, \omega)$, $\mathbf{W}_d^{(j)}(\xi, \eta, z_{j-1}, \omega)$ for L_j ($j = 2, 3, \ldots, n$) can be obtained using Eq. (35). After determining the wave vectors for an arbitrary layer via Eq. (35), the displacements, the stresses and the pore pressure can be evaluated by Eq. (26).

If the displacements, the stresses and the pore pressure of the half-space are denoted by the symbol $\hat{\tilde{\Omega}}(\xi, \eta, z, \omega)$, then, in view of Eq. (44), all the variables can be expressed in the following form:

$$\hat{\tilde{\Omega}}(\xi, \eta, z, \omega) = \delta(\omega + \xi c)\hat{\tilde{\Omega}}^*(\xi, \eta, z, \omega). \tag{48}$$

Thus, the displacements, the stresses and the pore pressure of the half-space in the time–space domain have the following uniform form:

$$\Omega(x,y,z,t) = \left(\frac{1}{2\pi}\right)^3 \int_{-\infty}^{+\infty}\int_{-\infty}^{+\infty}\int_{-\infty}^{+\infty} \delta(\omega + \xi c)\hat{\tilde{\Omega}}^*(\xi, \eta, z, \omega) e^{i(\omega t + \xi x + \eta y)}\, d\xi\, d\eta\, d\omega. \tag{49}$$

Due to the presence of Dirac's delta function in the above integral, the inversion of the Fourier transform with respect to ω in Eq. (49) can be accomplished analytically by simply replacing ω with $-\xi c$. As a result, the original triple integral is reduced to the following double integral with respect to the wavenumbers ξ, η:

$$\Omega(x,y,z,t) = \left(\frac{1}{2\pi}\right)^3 \int_{-\infty}^{+\infty}\int_{-\infty}^{+\infty} \hat{\tilde{\Omega}}^*(\xi, \eta, z, -\xi c) e^{i\xi(x-ct)} e^{i\eta y}\, d\xi\, d\eta. \tag{50}$$

It follows from Eq. (50) that the frequency composition of the response of the porous medium depends on the velocity of the moving load. Thus, for high-velocity moving loads, high frequency component is involved. Therefore, the low-frequency Biot's theory is not appropriate for treating moving loads with high speeds. To describe high-frequency drag force between the solid skeleton and the pore fluid, JKD model [20] is incorporated with Biot's theory in this study. According to JKD model, the frequency domain viscosity correction function corresponding to the time domain $K(t)$ in Eq. (4b) assumes the form:

$$\hat{K}(\omega) = \left(1 + i\frac{\omega}{\omega_c}a_g\right)^{1/2}, \quad \omega_c = \frac{b_p f}{\rho_f a_\infty}, \tag{51}$$

where ω_c is transition frequency which separates viscous-force-dominated flow from inertial-force-dominated flow and a_g is the pore geometry term which assumes $\frac{1}{2}$ for many porous media [20].

It also should be noted that the real ξ-axis and η-axis is free of any singularities for a multi-layered poroelastic medium if the parameter b_p representing internal friction between the solid and the pore fluid does

not vanish. Thus, the infinite integration in Eq. (50) with respect to the horizontal wavenumber ξ and η are free of any singularity in the path of integration. In this paper, the FFT method is used to conduct the inverse Fourier transform [22]. To avoid aliasing and leakage when conducting the inverse transform, the integrals with respect to wavenumber ξ and η must be truncated at sufficiently large values, and the sample spacing in wavenumber domain ξ and η must fulfill the following requirement:

$$\Delta\xi < \frac{1}{X_{\max}}, \quad \Delta\eta < \frac{1}{Y_{\max}}, \tag{52}$$

where $X_{\max}$ and $Y_{\max}$ specify the size of the domain over which the response of the half-space is non-vanishing. In this paper, we found that a discrete grid of 2045×2045 for the domain $-16\,\mathrm{m}^{-1} \leqslant \xi, \eta \leqslant 16\,\mathrm{m}^{-1}$ satisfies Eq. (52) and can ensure enough accuracy for the inversion of the Fourier transform.

6. Numerical results

6.1. Validation of the proposed method

When the material parameters for each layer are assumed the same values, the layered poroelastic half-space will be reduced to a homogeneous poroelastic half-space. As the first test, the results for the reduced homogeneous poroelastic half-space in this study will be compared with corresponding results in Ref. [11]. The half-space consists of three layers: two saturated porous layers and an underlying homogeneous porous half-space. The material parameters for the three layers take the following values: $\mu^{(1)} = \mu^{(2)} = \mu^{(3)} = 2.0 \times 10^7\,\mathrm{N/m^2}$, $\lambda^{(1)} = \lambda^{(2)} = \lambda^{(3)} = 4.0 \times 10^7\,\mathrm{N/m^2}$, $M^{(1)} = M^{(2)} = M^{(3)} = 2.4 \times 10^8\,\mathrm{N/m^2}$, $\rho_s^{(1)} = \rho_s^{(2)} = \rho_s^{(3)} = 2.0 \times 10^3\,\mathrm{kg/m^3}$, $\rho_f^{(1)} = \rho_f^{(2)} = \rho_f^{(3)} = 1.0 \times 10^3\,\mathrm{kg/m^3}$, $f^{(1)} = f^{(2)} = f^{(3)} = 0.125$, $\alpha^{(1)} = \alpha^{(2)} = \alpha^{(3)} = 0.97$, $b_p^{(1)} = b_p^{(0)} = b_p^{(3)} = 1.94 \times 10^6\,\mathrm{kg/m^3 s}$, $m^{(1)} = m^{(2)} = m^{(3)} = 1990\,\mathrm{kg/m^3}$. The moving line load F is normal to the beam and its velocity assumes the values $c = 0.2v_{\mathrm{SH}}$, $c = 0.88v_{\mathrm{SH}}$, $c = 1.3v_{\mathrm{SH}}$, respectively, where $v_{\mathrm{SH}} = \sqrt{\mu^{(1)}/\rho_s^{(1)}}$. The magnitude of the load is F_z. The parameters for the beam are as follows: $EI_z = 1.28 \times 10^9\,\mathrm{N\,m^2}$, $m_b = 7350\,\mathrm{kg/m}$, $a = 2.0\,\mathrm{m}$.

Fig. 2 shows the vertical displacement for the beam versus the coordinate x' ($-60\,\mathrm{m} \leqslant x' = x - ct \leqslant 60\,\mathrm{m}$) for the three cases: $c = 0.2v_{\mathrm{SH}}$, $c = 0.88v_{\mathrm{SH}}$, $c = 13v_{\mathrm{SH}}$, where the vertical displacement for the beam is normalized as $w_b^* = \mu_R w_b a_R / F_z$. The reference shear modulus, length is $\mu_R = 2.0 \times 10^7\,\mathrm{N/m^2}$, $a_R = 2.0\,\mathrm{m}$, respectively.

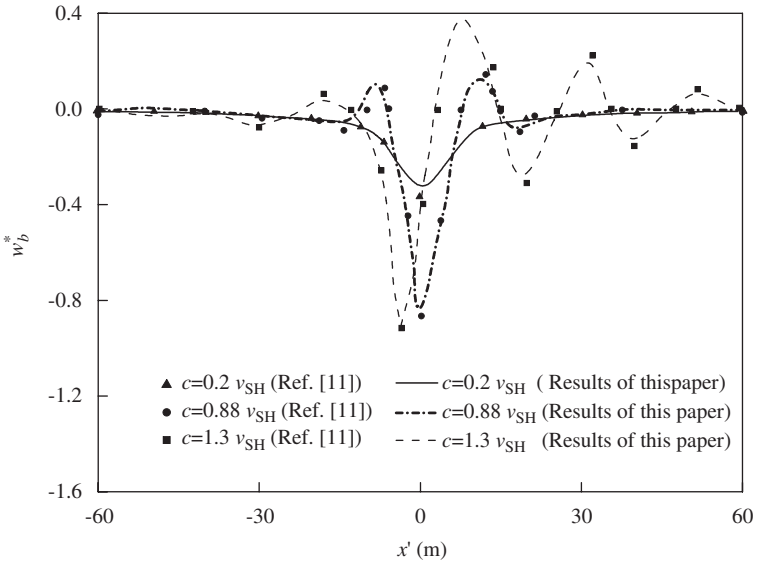

Fig. 2. Comparison of present vertical deflections of a beam overlying a homogeneous poroelastic half-space with results of Ref. [11] for different velocities: (a) $c = 0.2v_{\mathrm{SH}}$, (b) $c = 0.88v_{\mathrm{SH}}$ and (c) $c = 1.3v_{\mathrm{SH}}$.

In order to validate our method, results of Jin [11] are also shown in Fig. 2. It follows from Fig. 2 that results of the current paper are in a very good agreement with those of Jin [11].

6.2. Dynamic response of an infinite beam resting on a two-layered poroelastic half-space

In this section, the layered half-space consists of an upper layer and an underlying homogeneous half-space. The upper layer is a saturated poroelastic layer with depth h, while the lower half-space is a rigid bedrock with

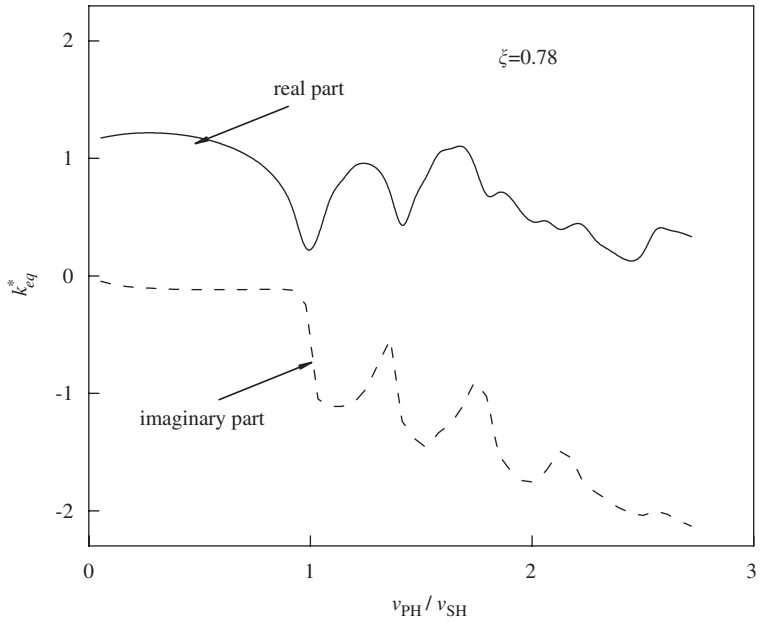

Fig. 3. The equivalent stiffness k^*_{eq} for a two-layer poroelastic half-space as a function of the phase velocity v_{PH} for wavenumber $\xi = 0.78$ m.

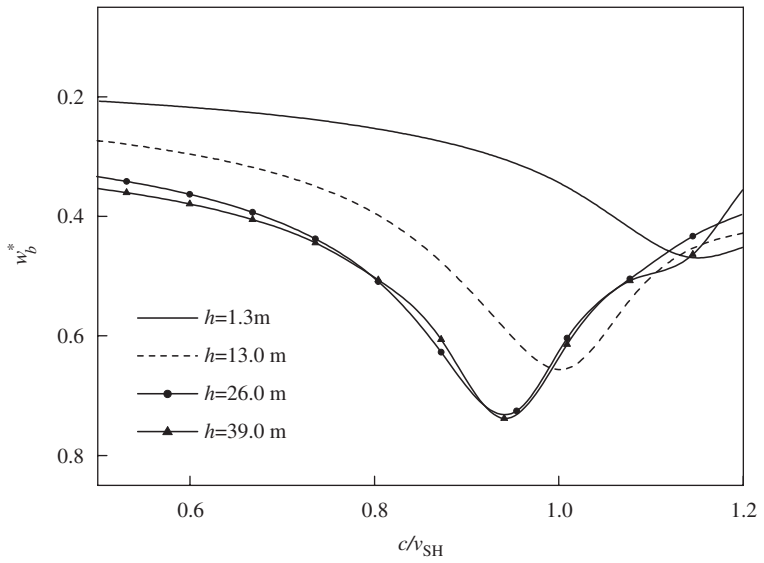

Fig. 4. The maximum vertical deflection of the beam w^*_b versus moving load velocity c for different depths of the overlying layer: (a) $h = 1.3$ m, (b) $h = 13.0$ m, (c) $h = 26.0$ m and (d) $h = 39.0$ m.

an impermeable surface. The line load F moves along the positive x-axis with a constant velocity c and the load is normal to the beam. In this example, the equivalent stiffness of the two-layered half-space is calculated first. Then, influences of the thickness of the upper layer on the vertical vibration and the internal forces of the beam are discussed.

The parameters for the beam and the upper layer are given as follows: $EI_z = 1.3 \times 10^9\,\mathrm{N\,m^2}$, $m_b = 1770\,\mathrm{kg/m}$, $a = 1.3\,\mathrm{m}$, $\mu = 3.8 \times 10^7\,\mathrm{N/m^2}$, $\lambda = 3.8 \times 10^7\,\mathrm{N/m^2}$, $M = 2.4 \times 10^8\,\mathrm{N/m^2}$, $\rho_s = 2.0 \times 10^3\,\mathrm{kg/m^3}$, $\rho_f = 1.0 \times 10^3\,\mathrm{kg/m^3}$, $f = 0.35$, $\alpha = 0.97$, $b_p = 1.94 \times 10^6\,\mathrm{kg/m^3 s}$, $m = 1990\,\mathrm{kg/m^3}$.

To analyze k_{eq} the following variables are introduced: the phase velocity $v_{\mathrm{PH}} = \omega/\xi$ of waves in the beam and a reference shear wave velocity which is defined as $v_{\mathrm{SH}} = \sqrt{\mu/\rho_s}$. The equivalent stiffness k_{eq} is normalized as $k^*_{\mathrm{eq}} = k_{\mathrm{eq}}/\mu$. Moreover, the vertical displacement, the bending moment and the shear force of the beam are normalized as $w^*_b = \mu w_b a/F_z$, $M^* = M_x/(F_z a)$, $Q^* = Q_x/F_z$, respectively.

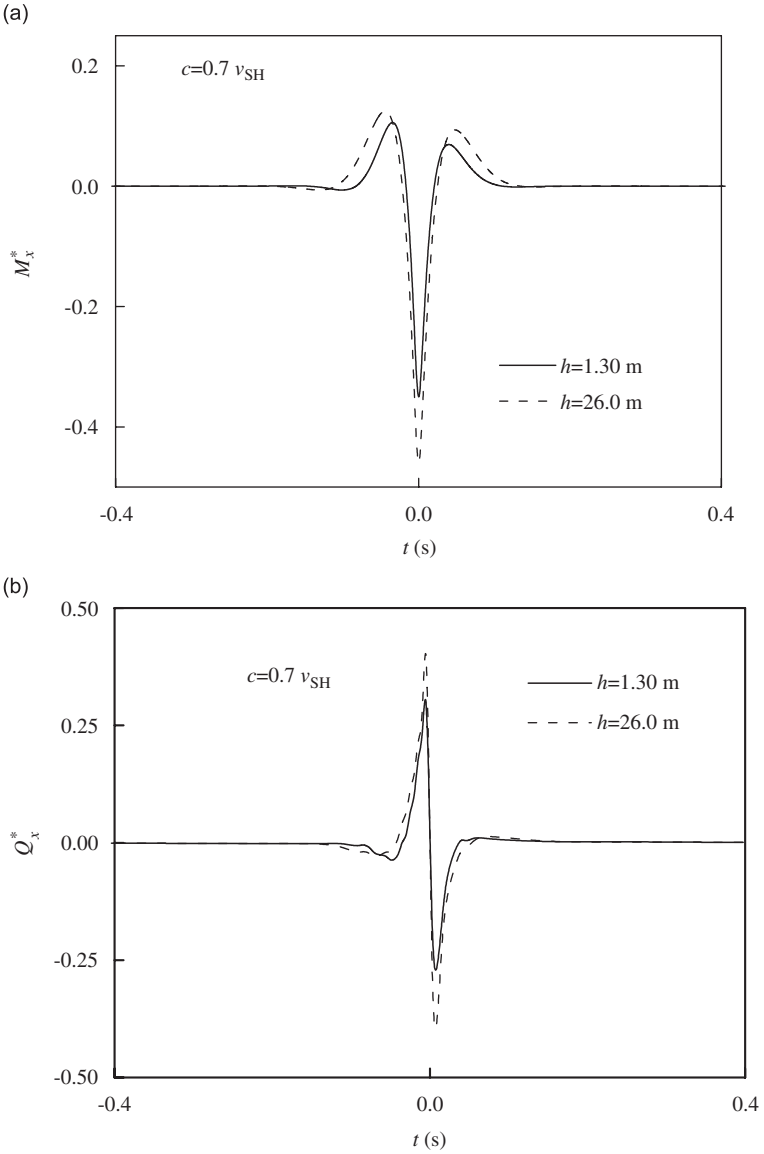

Fig. 5. The internal force for the infinite beam subjected to a moving load with a constant velocity $c = 0.7v_{\mathrm{SH}}$ at the observation point $P(0.0\,\mathrm{m})$ versus time t for two depths of the overlying layer, $h = 1.3$ and $26.0\,\mathrm{m}$: (a) the bending moment versus time t; (b) the shear force versus time t.

6.2.1. The equivalent stiffness of the two-layered poroelastic half-space

The equivalent stiffness k_{eq} of the half-space is a function of the frequency ω and the wavenumber ξ, which can be obtained by performing integration with respect to the wavenumber η. As the real η axis is free of any singularities for a layer poroelastic half-space due to the attenuation of the porous medium, thus, the integral in Eq. (45) can be evaluated by a direct numerical integration. In calculation, the thickness of the upper porous layer is $h = 10.4$ m.

Fig. 3 depicts the equivalent stiffness k^*_{eq} as a function of the phase velocity v_{PH} for wavenumber $\xi = 0.78$ m. It follows from Fig. 3 that for $v_{PH} < v_{CR}$, the imaginary part of the equivalent stiffness is very small; however, for $v_{PH} > v_{CR}$, the imaginary part of the stiffness increases considerably, where v_{CR} is the critical velocity [7]. The significant increase of the imaginary part of the stiffness when $v_{PH} > v_{CR}$ is due to the radiation of energy into the half-space, which takes energy from the beam and entails substantial attenuation for the motion of the beam. Besides, Fig. 3 suggests that the equivalent stiffness becomes rather small (both the real and the imaginary part) for $v_{PH} = v_{CR}$, which is mainly due to the resonance of the system [7]. Moreover, both the real and the imaginary part of the equivalent stiffness has a set of minima when $v_{PH} > v_{CR}$. Therefore, for the beam on a layered poroelastic half-space, there still exist critical velocities even when the load velocity is larger than the shear wave speed of the medium. According to Metrikine and Popp [7], the critical (resonance) velocity of the moving load can be determined from the curves of the lowest dispersion branch of the layer. In this section, for the upper layer with depth $h = 10.4$ m, the critical velocity is $v_{CR} = 0.97 v_{SH}$, which is very close to the Rayleigh wave velocity v_R of the porous medium.

6.2.2. The influences of the thickness of the upper layer on the response of the beam

In the following calculation, thickness of the upper porous layer assumes the values $h = 1.3$, 13.0, 26.0 and 39.0 m. The maximum vertical deflection of the beam w^*_b versus the moving load velocity c/v_{SH} is shown in Fig. 4 for different depths. Fig. 4 shows that at first the maximum deflection of the beam increases as the depth of the upper layer increases. However, when the depth reaches $h = 26.0$ m, the increment is very small.

Figs. 5(a) and (b) illustrate the bending moment and the shear force for the infinite beam at the observation point $P(0.0\,\text{m}, 0.0\text{m})$ versus time t for two depths of the layer: $h = 1.3$ and 26.0 m. The velocity of the moving load is $c = 0.7 v_{SH}$. Time $t = 0.0$ s corresponds to the instant at which the moving load is located at the origin. Fig. 5 shows that the increasing thickness of the layer enhances the bending moment and the shear force of the beam markedly.

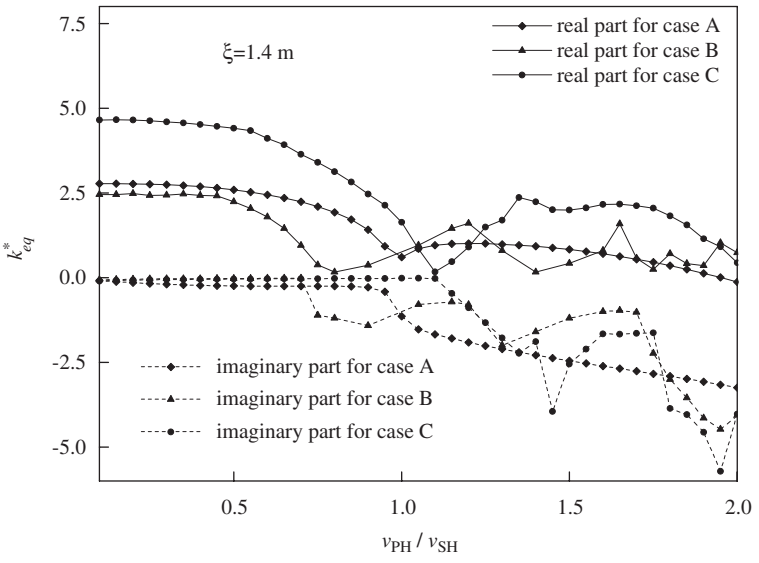

Fig. 6. The equivalent stiffness k^*_{eq} for a three-layer poroelastic half-space as a function of the phase velocity v_{PH} for wavenumber $\xi = 1.4$ m.

6.3. Dynamic response of an infinite beam resting on a three-layered poroelastic half-space

In this example, the infinite beam is assumed to rest on a three-layer poroelastic half-space, which consists of two saturated porous layers and an underlying homogeneous porous half-space. The line normal load F moves along the positive x-axis direction with a constant velocity c. The thicknesses of the upper two layers are $h^{(1)} = h^{(2)} = 2.0\,\mathrm{m}$. The Lame constants of the three layers for cases A–C assume the following values: (A) $\mu^{(1)}{:}\mu^{(2)}{:}\mu^{(3)} = \lambda^{(1)}{:}\lambda^{(2)}{:}\lambda^{(3)} = 1{:}1{:}1$; (B) $\mu^{(1)}{:}\mu^{(2)}{:}\mu^{(3)} = \lambda^{(1)}{:}\lambda^{(2)}{:}\lambda^{(3)} = 1{:}0.2{:}1$; (C) $\mu^{(1)}{:}\mu^{(2)}{:}\mu^{(3)} = \lambda^{(1)}{:}\lambda^{(2)}{:}\lambda^{(3)} = 1{:}5{:}1$, where $\mu^{(3)} = 2.5 \times 10^7\,\mathrm{N/m^2}$, $\lambda^{(3)} = 5.0 \times 10^7\,\mathrm{N/m^2}$. The remaining parameters for each layer take the following values: $m^{(1)} = m^{(2)} = m^{(3)} = 1990\,\mathrm{kg/m^3}$, $\rho_s^{(1)} = \rho_s^{(2)} = \rho_s^{(3)} = 2.0 \times 10^3\,\mathrm{kg/m^3}$, $\rho_f^{(1)} = \rho_f^{(2)} = \rho_f^{(3)} =$

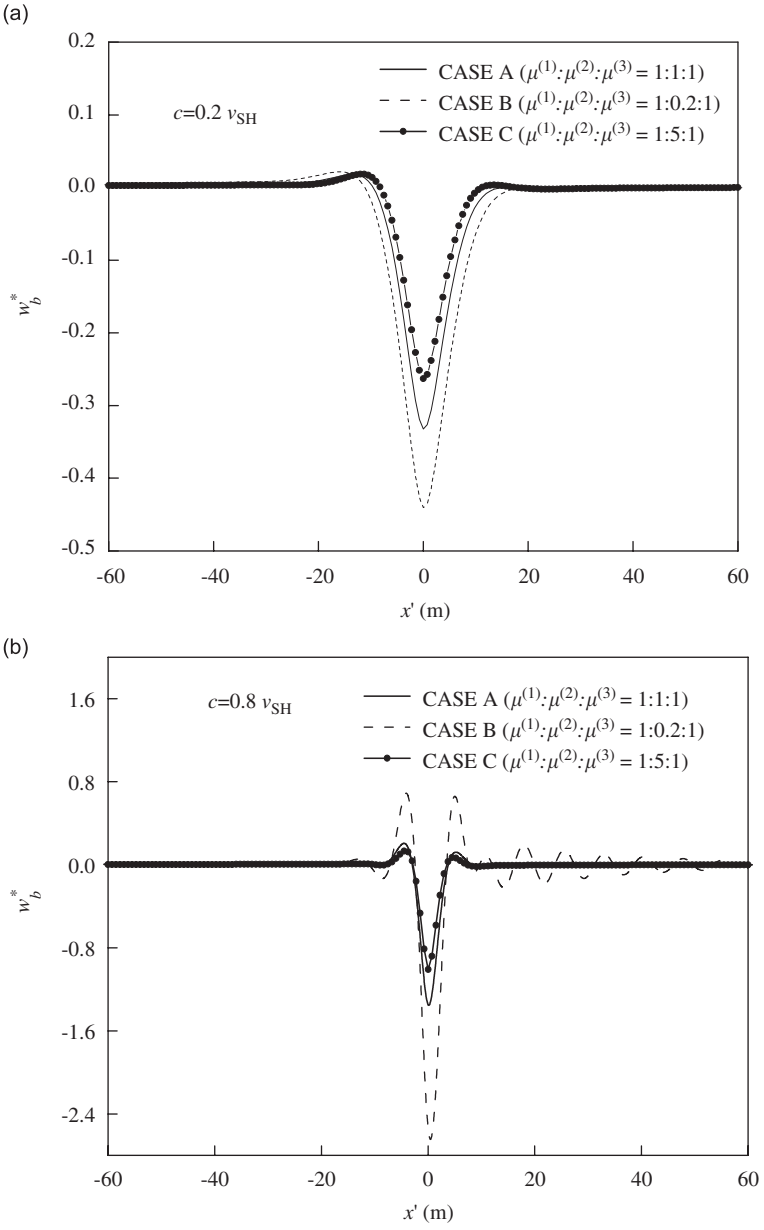

Fig. 7. The deflection w_b^* versus coordinates $-60.0\,\mathrm{m} \leqslant x' = x - ct \leqslant 60.0\,\mathrm{m}$ for the beam subjected to a moving load: (a) velocity $c = 0.2v_{\mathrm{SH}}$; (b) velocity $c = 0.8v_{\mathrm{SH}}$.

$1.0 \times 10^3\,\mathrm{kg/m^3}$, $f^{(1)} = f^{(2)} = f^{(3)} = 0.3$, $\alpha^{(1)} = \alpha^{(2)} = \alpha^{(3)} = 0.97$, $M^{(1)} = M^{(2)} = M^{(3)} = 5.0 \times 10^9\,\mathrm{N/m^2}$, $b_p^{(1)} = b_p^{(2)} = b_p^{(3)} = 1.0 \times 10^{10}\,\mathrm{kg/m^3\,s}$. The parameters for the beam are as follows: $EI_z = 1.2 \times 10^9\,\mathrm{N\,m^2}$, $m_b = 1790\,\mathrm{kg/m}$, $a = 2.0\,\mathrm{m}$. The reference shear wave velocity is defined as $v_{\mathrm{SH}} = \sqrt{\mu^{(3)}/\rho_s^{(3)}}$.

6.3.1. The equivalent stiffness of the three-layered poroelastic half-space

To analyze the equivalent stiffness k_{eq} of the three-layered poroelastic half-space, the same phase velocity $v_{\mathrm{PH}} = \omega/\xi$ as in Section 6.2 is also introduced. The equivalent stiffness is normalized as $k_{\mathrm{eq}}^* = k_{\mathrm{eq}}/\mu_R$, the reference shear modulus is $\mu_R = 2.5 \times 10^7\,\mathrm{N/m^2}$.

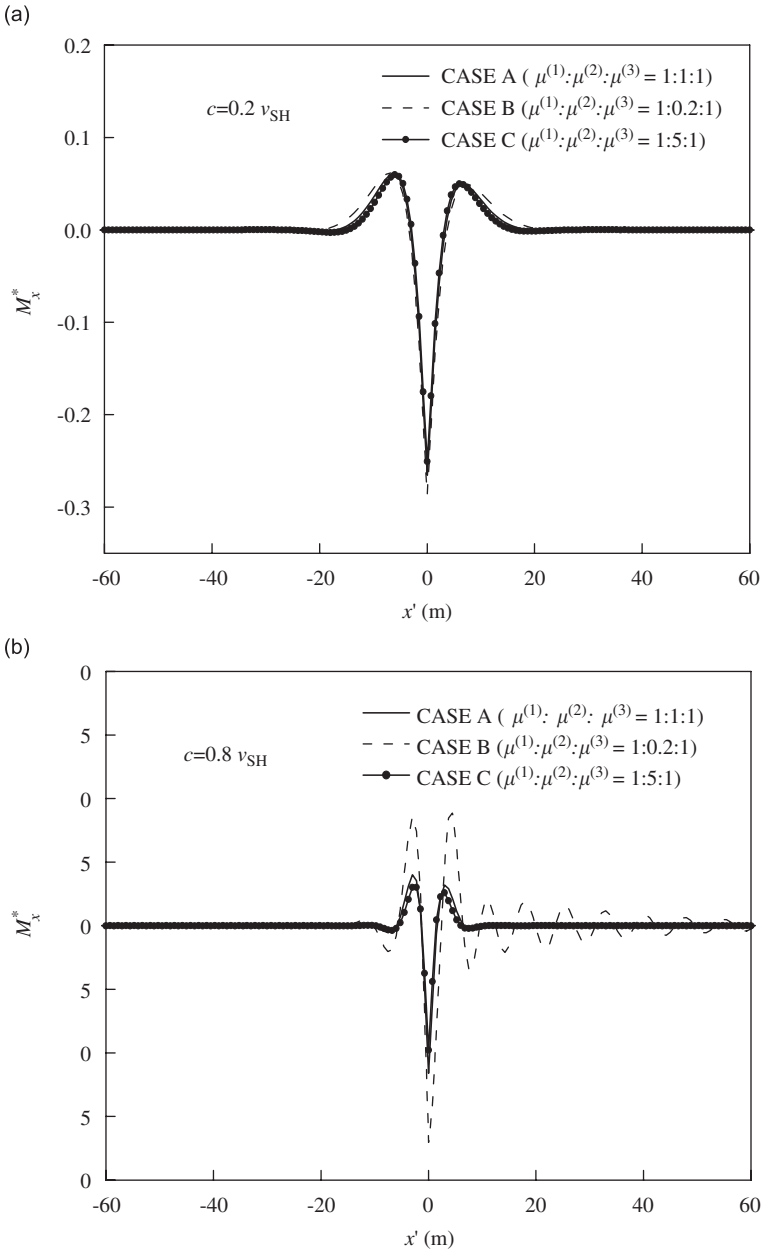

Fig. 8. The bending moment M_x^* versus the coordinates $-60.0\,\mathrm{m} \leqslant x' = x - ct \leqslant 60.0\,\mathrm{m}$ for the beam subjected to a moving load: (a) velocity $c = 0.2v_{\mathrm{SH}}$; (b) velocity $c = 0.8v_{\mathrm{SH}}$.

Fig. 6 depicts the equivalent stiffness of the three-layered poroelastic half-space for wavenumber $\xi = 1.4\,\mathrm{m}$. According to the method outlined in Ref. [7], the critical velocities v_{CR} for the three cases are obtained as follows: $v_{CR} = 0.94v_{SH}$ for case A; $v_{CR} = 0.85v_{SH}$ for case B; $v_{CR} = 1.09v_{SH}$ for case C. Fig. 6 shows for $v_{PH} < 0.85v_{SH}$, the real part of the equivalent stiffness of case C is larger than those for the other two cases.

6.3.2. Dynamic response of the beam resting on the three-layered poroelastic half-space

In this part, results for the vertical displacements, the bending moment and the shear force for the beam are given and are normalized as $w_b^* = \mu_R w_b a_R/F_z$, $M_x^* = M_x/(F_z a_R)$, $Q_x^* = Q_x/F_z$. The reference shear modulus and the reference length are $\mu_R = 2.5 \times 10^7\,\mathrm{N/m^2}$ and $a_R = 2.0\,\mathrm{m}$, respectively.

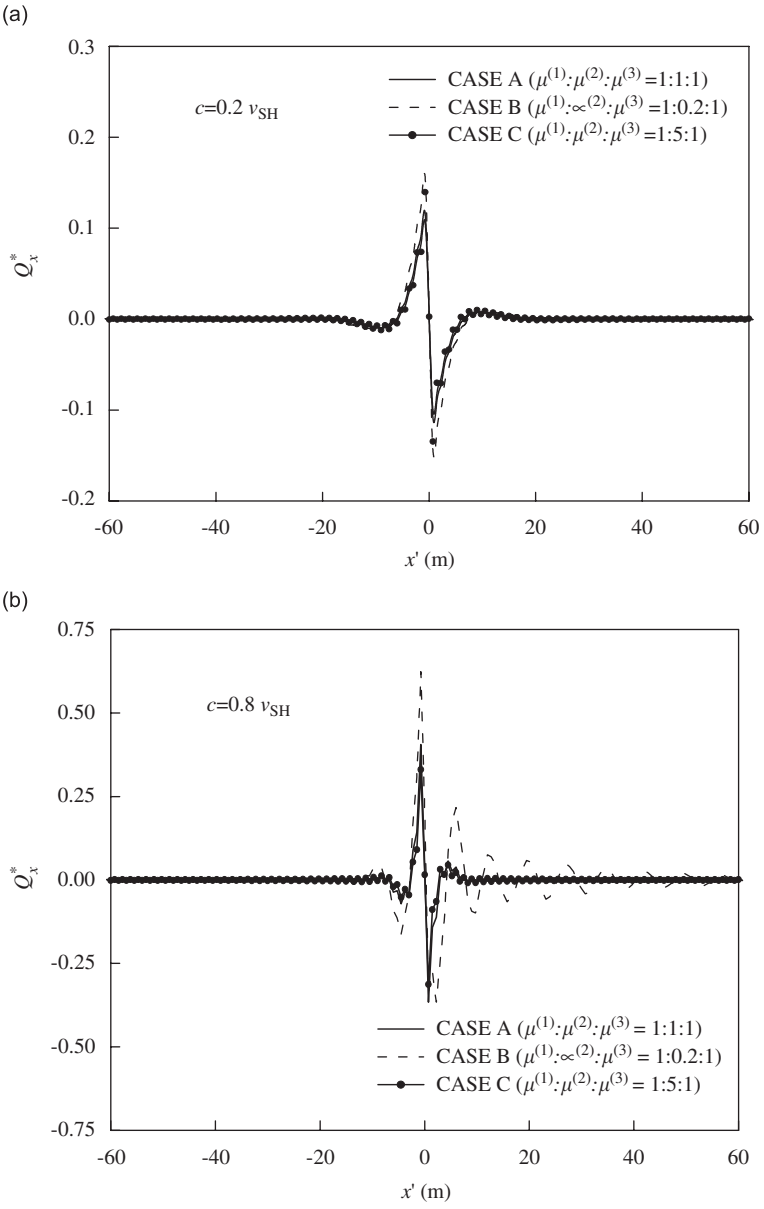

Fig. 9. The shear force Q_x^* versus coordinates $-60.0\,\mathrm{m} \leqslant x' = x - ct \leqslant 60.0\,\mathrm{m}$ for the beam subjected to a moving load: (a) velocity $c = 0.2v_{SH}$; (b) velocity $c = 0.8v_{SH}$.

Figs. 7–9 show the vertical displacements, the bending moment and the shear force of the beam versus the coordinate $-60.0\,\mathrm{m} \leqslant x' = x - ct \leqslant 60.0\,\mathrm{m}$. In calculation, the moving load is located at point ($x' = 0.0\,\mathrm{m}$) with velocity $c = 0.2v_{\mathrm{SH}}$, $c = 0.8v_{\mathrm{SH}}$, respectively. For velocity $c = 0.2v_{\mathrm{SH}}$, the vertical displacement, the bending moment and the shear force of the beam are almost symmetrical with respect to the point $x' = 0.0\,\mathrm{m}$; however, for velocity $c = 0.8v_{\mathrm{SH}}$, the symmetry with respect to the point $x' = 0.0\,\mathrm{m}$ is broken. Also, Figs. 7–9 illustrate that the presence of a softer middle layer within the layered half-space leads to a considerable increment of the vertical displacement, the bending moment and the shear force, which is more pronounced for the case $c = 0.8v_{\mathrm{SH}}$. Also, the softer middle layer makes the responses of the infinite beam oscillate dramatically.

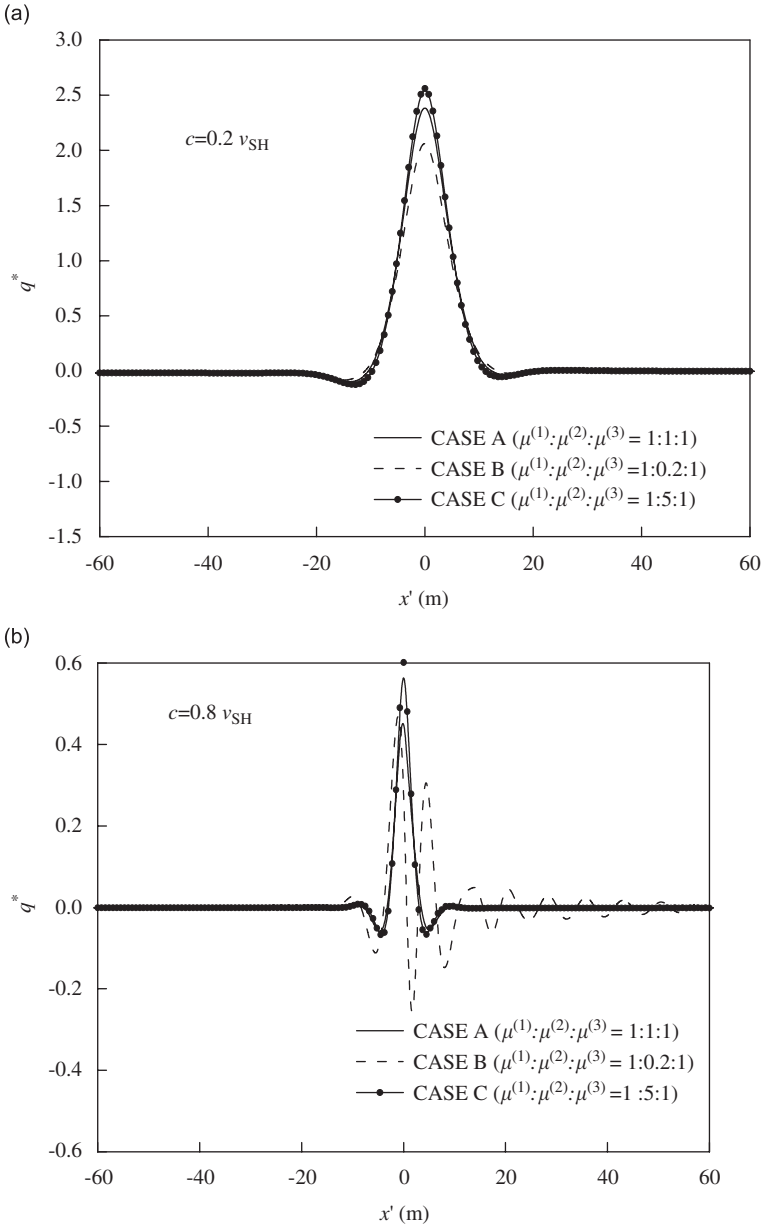

Fig. 10. The interaction force q^* between the beam and a three-layered poroelastic half-space for coordinate $-60.0\,\mathrm{m} \leqslant x' = x - ct \leqslant 60.0\,\mathrm{m}$: (a) velocity $c = 0.2v_{\mathrm{SH}}$; (b) velocity $c = 0.8v_{\mathrm{SH}}$.

6.4. Soil response due to moving loads

In this example, the parameters for the half-space and the beam take the same values as in Section 6.3. The contact force between the beam and the half-space and pore pressure of the half-space due to moving load will be calculated. The moving line load is located at point ($x' = 0.0$ m) with the velocity $c = 0.2v_{SH}$, $c = 0.8v_{SH}$, respectively. The contact force and the pore pressure are normalized as $q^* = qa_R/F_z$, $p^* = pa_R^2/F_z$, respectively. The reference length is chosen as $a_R = 2.0$ m.

Fig. 10 illustrates the contact force between the beam and the half-space surface versus the coordinate $-60.0\,\text{m} \leqslant x' = x - ct \leqslant 60.0\,\text{m}$ with $y = z = 0.0$ m. For velocity $c = 0.2v_{SH}$, the contact force is almost symmetrical with respect to the point $x' = 0.0$ m; however, for velocity $c = 0.8v_{SH}$, the symmetry is lost.

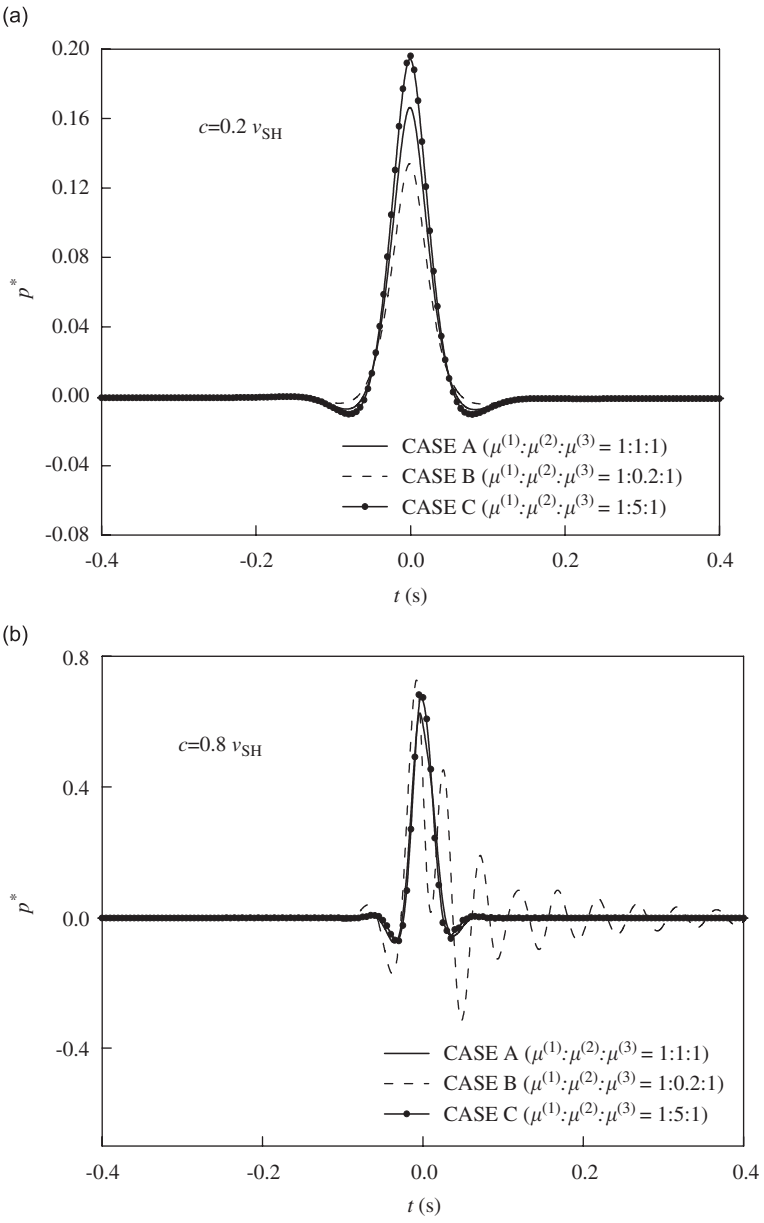

Fig. 11. The pore pressure p^* at the observation point $P(0.0\,\text{m}, 1.0\,\text{m}, 2.0\,\text{m})$ due to a moving load applied on the beam overlying a three-layered poroelastic half-space: (a) velocity $c = 0.2v_{SH}$; (b) velocity $c = 0.8v_{SH}$.

Comparing Fig. 10 with Figs. 8 and 9, it is observed that the softer middle layer diminishes the contact force between the half-space and the beam.

Fig. 11 plots the pore pressure for the soil at the point $P(x = 0.0, 1.0$ and $2.0\,\mathrm{m})$ versus time t. Likewise, time $t = 0.0\,\mathrm{s}$ corresponds to the instant at which the applied load passing through the origin. It follows from Fig. 11 that for all the three cases, the pore pressure at the observation point increases with increasing velocity. One can also see that the presence of a softer middle layer enhances the pore pressure for the case $c = 0.8v_{\mathrm{SH}}$, while it diminishes the pore pressure for the case $c = 0.2v_{\mathrm{SH}}$. From Fig. 11(a), one can see that for lower velocity ($c = 0.2v_{\mathrm{SH}}$), the pore pressure is symmetrical with respect to time $t = 0.0\,\mathrm{s}$. However, for larger velocity ($c = 0.8v_{\mathrm{SH}}$), the symmetry is missing (Fig. 11(b)). Furthermore, negative pore pressure occurs at time around $t = 0.0\,\mathrm{s}$.

7. Conclusions

Dynamic response of an infinite beam resting on a layered poroelastic half-space subjected to moving loads is addressed in this study. The equivalent stiffness of the layered porous half-space is derived by means of the TRM method. Based on the proposed methodology, the deflection, the bending moment and the shear force of the beam are obtained. Response of the half-space due to moving loading is also calculated. The influences of the load speed and parameters of the poroelastic half-space on the beam responses are investigated. It follows from the numerical results that the presence of a softer middle layer inside the layered half-space leads to a considerable increment of the vertical displacement, the bending moment and the shear force, in particular for high velocity cases. Also, the middle softer layer makes the responses of the infinite beam oscillate dramatically. The present investigation also shows that for a beam overlying a layered poroelastic half-space, there still exist critical velocities even when the load velocity is larger than the shear wave velocity of the medium.

Acknowledgments

The project is supported by the National Natural Science Foundation of China with Grant No. 50578071.

References

[1] A.V. Metrikine, H.A. Dieterman, Three-dimensional vibrations of a beam on and elastic half-space: resonance interaction of vertical longitudinal and lateral beam waves, *Journal of Applied Mathematics and Mechanics* 64 (1997) 951–956.
[2] A.B. Lipen, A.V. Chigarev, The displacements in an elastic half-space when a load moves along a beam lying on its surface, *Journal of Applied Mathematics and Mechanics* 62 (5) (1998) 791–796.
[3] X. Sheng, C.J.C. Jones, M. Petyt, Ground vibration generated by a harmonic load acting on a railway track, *Journal of Sound and Vibration* 225 (1) (1999) 3–28.
[4] C. Madshus, A.M. Kaynia, High-speed railway lines on soft ground: dynamic behavior at critical train speed, *Journal of Sound and Vibration* 231 (3) (2000) 689–701.
[5] H. Takemiya, Simulation of track-ground vibrations due to a high-speed train: the case of X-2000 at Ledsgard, *Journal of Sound and Vibration* 261 (2003) 503–526.
[6] M.H. Kargarnovin, D. Younesian, Dynamics of Timoshenko beams on Pasternak foundation under moving load, *Mechanics Research Communications* 31 (2004) 713–723.
[7] A.V. Metrikine, K. Popp, Steady-state response of an elastic beam on a visco-elastic layer under moving load, *Archive of Applied Mechanics* 70 (2000) 399–408.
[8] A.V. Vostroukhov, A.V. Metrikine, Periodically supported beam on a visco-elastic layer as a model for dynamic analysis of a high-speed railway track, *International Journal of Solids and Structures* 40 (2003) 5723–5752.
[9] L. Auersch, The excitation of ground vibration by rail traffic: theory of vehicle–track–soil interaction and measurements on high-speed lines, *Journal of Sound and Vibration* 284 (2005) 103–132.
[10] L. Auersch, Dynamics of the railway track and the underlying soil: the boundary-element solution, theoretical results and their experimental verification, *Vehicle System Dynamics* 43 (9) (2005) 671–695.
[11] B. Jin, Dynamic displacement of an infinite beam on a poroelastic half space due to a moving oscillating load, *Archive of Applied Mechanics* 74 (2004) 277–287.
[12] M.A. Biot, Theory of propagation of elastic waves in a fluid-saturated porous solid, I: Low frequency range, *Journal of the Acoustical Society of America* 28 (1956) 168–178.

[13] M.A. Biot, Theory of propagation of elastic waves in a fluid-saturated porous solid, II: Higher frequency range, *Journal of the Acoustical Society of America* 28 (1956) 179–191.
[14] M.A. Biot, Mechanics of deformation and acoustic propagation in porous media, *Journal of Applied Psychology* 33 (1962) 1482–1498.
[15] J.F. Lu, A. Hanyga, Fundamental solution for a layered porous half space subject to a vertical point force or a point fluid source, *Computational Mechanics* 35 (5) (2005) 376–391.
[16] J.E. Luco, R.J. Apsel, On the Green's functions for a layered half-space: Part I, *Bulletin of the Seismological Society of America* 73 (1983) 909–929.
[17] R.J. Apsel, J.E. Luco, On the Green's functions for a layered half-space: Part II, *Bulletin of the Seismological Society of America* 73 (1983) 931–951.
[18] X.F. Chen, Seismogram synthesis for multi-layered media with irregular interfaces by global generalized reflection/transmission matrices method 3: Theory of 2D P-SV case, *Bulletin of the Seismological Society of America* 86 (1996) 389–405.
[19] R.Y.S. Pak, B.B. Guzina, Three-dimensional Green's functions for a multilayered half-space in displacement potentials, *Journal of Engineering Mechanics* 128 (2002) 449–461.
[20] D.L. Johnson, J. Koplik, R. Dashen, Theory of dynamic permeability and tortuosity in fluid-saturated porous-media, *Journal of Fluid Mechanics* 176 (1987) 379–402.
[21] H. Deresiewicz, R. Skalak, On the uniqueness in dynamic poroelasticity, *Bulletin of the Seismological Society of America* 53 (1963) 783–788.
[22] A.V. Oppenheim, R.W. Schafer, *Discrete-time Signal Processing*, Prentice-Hall, Inc., Englewood Cliffs, NJ, 1999.